Space–Time Selective RAKE Receiver With Finger Selection Strategies for UWB Overlay Communications

Tsung-Hui Chang, Chong-Yung Chi, *Senior Member, IEEE*, and Yu-Jung Chang

***Abstract*—This paper proposes a space–time selective RAKE (SRAKE) receiver with maximum signal-to-interference-plus-noise ratio (MSINR) for direct-sequence ultra-wideband (UWB) communications in the presence of narrowband interference (NBI) and multiple-access interference. For effectively extracting a fixed number of the UWB signal components (fingers) from numerous resolvable paths, four finger selection strategies (FSSs) are considered for the proposed space-time SRAKE receiver, including the optimum FSS (with MSINR), which is not very computationally feasible, and three feasible FSSs: an energy-based FSS (EB-FSS), a constrained energy-based FSS (CEB-FSS), and a hybrid energy-based FSS, which is also a combination of the EB-FSS and CEB-FSS. Through a performance analysis, we show that the performance of the proposed receiver in the presence of NBI not only depends on the power ratio, bandwidth ratio, and relative spectrum location of NBI with respect to the UWB signal, but also on the FSS used. Some simulation results are then presented to show that the proposed space–time MSINR-SRAKE receiver with the preceding FSSs used can provide a larger system capacity and better immunity to strong NBI than the existing time-only SRAKE receivers and space–time SRAKE receivers.**

***Index Terms*—Finger selection strategy (FSS), narrowband interference (NBI), RAKE receiver, selective RAKE (SRAKE) receiver, signal-to-interference-plus-noise ratio (SINR), space–time RAKE receiver, ultra-wideband (UWB).**

I. Introduction

RECENTLY, ultra-wideband (UWB) systems have drawn extensive attention in wireless indoor communications due to unique features of high data rate in short distance, reduced fading effect per resolvable path, low-power transmission, and low design complexity. The Federal Communication Commission (FCC) released huge bandwidth over 3.1–10.6 GHz for UWB communications overlaying existing narrowband systems operating with low-power (less than -41.3 dBm/MHz) ultrashort pulses [1]. In addition to multiple-access interference (MAI) from other active UWB users, the existing systems operating with much narrower bandwidth cause strong narrowband interference (NBI) to the UWB receiver. Therefore, the UWB system design is challenging because of the presence of both NBI and MAI [2].

Due to fine delay resolution of UWB pulses, the UWB signal energy is distributed over a large number of component paths. The RAKE-based receivers can be used to capture the desired signal energy from numerous paths and meanwhile can achieve multipath diversity through maximum ratio combining (MRC) [2]. However, the conventional all-RAKE receiver, which collects all of the resolvable path components, is not feasible for UWB systems due to extraordinary complexity resulting from too many resolvable paths. Therefore, selective RAKE (SRAKE) receivers have been considered, which only extract signal components from a subset of all of the resolvable paths [3]–[5]. An efficient finger selection strategy (FSS) for SRAKE receivers in UWB multipath channels is crucial to the optimal tradeoff of receiver complexity and performance [5]. Win *et al.* [5] reported the performance of SRAKE receivers with MRC (MRC-SRAKE) for UWB communication systems using an FSS of selecting a certain number of either the strongest or first arriving paths. Klein *et al.* [6], using the FSS by minimum mean-square error (MMSE) between the RAKE output and the desired symbol, and Boubaker and Letaief [7], using the same FSSs as reported in [5], further proposed SRAKE receivers with MMSE combining (MMSE-SRAKE) for time-hopping UWB (TH-UWB) systems, specifically for the narrowband intereference (NBI) suppression.

It is well known that receivers with multiple antennas can increase degrees of freedom for interference cancellation and diversity combining. The performance of the space–time MRC-SRAKE receiver (with the same MRC-SRAKE used at each receive antenna) of TH-UWB systems reported in [8] shows that the multiple-access capability of UWB systems can be significantly improved by exploiting spatial and multipath diversity, but the effect of NBI upon the space–time receiver was not considered yet. In conventional CDMA systems, the space–time RAKE receivers for interference suppression have been widely studied, e.g., [9]–[12] for MAI suppression and [13]–[15] for joint MAI and NBI suppression, but all of them concentrate on the all-RAKE structure. Obviously, the SRAKE is much preferable to the all-RAKE for UWB systems due to too many resolvable paths. Using the SRAKE instead of the all-RAKE, the paper proposes a space-time SRAKE receiver with maximum signal to interference-plus-noise ratio (MSINR) combining, referred to as the *space-time MSINR-SRAKE receiver*, for direct-sequence UWB (DS-UWB) communication systems.

Manuscript received August 10, 2005; revised January 4, 2006. This work was supported in part by the National Science Council, R.O.C., under Grant NSC 93-2213-E-007-079 and by the Industrial Technology Research Institute under Grant S5-930001. This work was presented in part at the IEEE International Conference on UWB, Zurich, Switzerland, Sept. 5–8, 2005.

T.-H.Chang and C.-Y. Chi are with the Department of Electrical Engineering and the Institute of Communications Engineering, National Tsing Hua University, Hsinchu 30013, Taiwan, R.O.C. (e-mail: cychi@ee.nthu.edu.tw).

Y.-J. Chang is with Accton Inc., Hsinchu 30077, Taiwan, R.O.C.

Digital Object Identifier 10.1109/TMTT.2006.871996

As SRAKE receivers, a proper FSS is needed by the proposed space-time MSINR-SRAKE receiver, whereas, in contrast to the one-dimensional (1-D) selection strategy used by time-only SRAKE receivers, the FSS is a two-dimensional (2-D) (space and time) selection strategy. In the paper, four FSSs are considered, including the optimum FSS (Opt-FSS), an energy-based FSS (EB-FSS), a constrained energy-based FSS (CEB-FSS), and a hybrid EB-FSS (HEB-FSS). A performance analysis of the proposed space–time MSINR-SRAKE receiver is also presented to show the dependence of the receiver performance (output SINR) not only upon the power ratio, bandwidth ratio, and relative spectrum location of NBI with respect to the UWB signal, but also upon the FSS used. The Opt-FSS can achieve the best receiver performance but involves formidable computational complexity. With feasible computational complexity, the EB-FSS, which is the direct extension of the one used by time-only SRAKE receivers [3]–[5], is only suitable for the case of weak NBI, and the CEB-FSS is suitable for the case of strong NBI. Therefore, the HEB-FSS, which is the combination of the EB-FSS and CEB-FSS, is suitable for a variety of NBI. Finally, some simulation results were presented to justify the efficacy of the proposed space–time MSINR-SRAKE receiver and the proposed four FSSs together with a comparison with time-only SRAKE receivers (including MRC-SRAKE [5] and MMSE-SRAKE [7]) and the space–time MRC-SRAKE receiver [8].

The remainder of this paper is organized as follows. The signal model of a multi-user DS-UWB system in an indoor overlay environment is presented in Section II. The proposed space–time MSINR-SRAKE receiver and the associated performance analysis in the presence of a single NBI are presented in Section III. Section IV presents the proposed four FSSs together with the associated performance analyses. Some simulation results are then provided in Section V. Finally, the conclusions are drawn in Section VI.

II. Signal Model

Consider the uplink transmission of a DS-UWB communication system in an indoor overlay environment. The public access point (i.e., base station) equipped with multiple antennas receives the signals from K DS-UWB portable units and an interfering signal from a narrowband device. The equivalent baseband signal transmitted by the jth DS-UWB portable unit can be represented as

$$s_j(t) = \sqrt{E_j} \sum_{k=-\infty}^{\infty} d_j[k] v_j(t - kT_s), \qquad j = 1, 2, \ldots, K \tag{1}$$

where E_j is the symbol energy, $d_j[k] \in \{-1, 1\}$ is the BPSK symbol, T_s is the symbol interval, and $v_j(t)$ is the symbol signature waveform with unity energy given by

$$v_j(t) = \sum_{i=0}^{P-1} c_j[i] \psi(t - iT_c) \tag{2}$$

where $c_j[i] \in \{1/\sqrt{P}, -1/\sqrt{P}\}$, $i = 0, 1, \ldots, P-1$, is the normalized spreading sequence of the jth user, $T_c = T_s/P$ denotes the chip interval, and $\psi(t)$ is the pulse-shaping function.

Suppose that the public access point is equipped with M sufficiently separated antenna elements such that the UWB signal received by each receive antenna experiences an independent channel fading. Assuming that the passband bandwidth of the UWB signal is $1/T_c$, the equivalent baseband tapped-delay-line channel model [13], [16], [17] from the jth DS-UWB user to antenna m is given by

$$h_m^{(j)}(t) = \sum_{\ell=0}^{L_j-1} g_{m,\ell}^{(j)} \delta(t - \ell T_c - \tau_j), \qquad m = 1, 2, \ldots, M \tag{3}$$

where $g_{m,\ell}^{(j)}$ is the complex-valued channel coefficient, L_j is the number of resolvable paths,[1] $\tau_j \in [0, T_c)$ denotes the fractional delay offset of the jth user, and $\delta(t)$ is the Dirac delta function.

The NBI received at the mth receive antenna can be modeled as [14]

$$\mathrm{i}_m(t) = \sqrt{J} a_m b(t) e^{j2\pi f_o t} \tag{4}$$

where J is the average power of the NBI, a_m is the NBI's complex channel coefficient with $\mathrm{E}\{|a_m|^2\} = 1$ (where $\mathrm{E}\{\cdot\}$ stands for the expectation operator), f_o is the offset between the carrier frequencies of the NBI and the UWB signal, and $b(t)$ is wide-sense stationary with zero mean, $\mathrm{E}\{|b(t)|^2\} = 1$, and power spectral density [18]

$$S_b(f) = \begin{cases} \frac{1}{B}, & |f| \le \frac{B}{2} \\ 0, & \text{otherwise} \end{cases} \tag{5}$$

where B is the passband bandwidth of $b(t)$.

As a result, the received low-pass signal at the mth receive antenna is given as follows:

$$y_m(t) = \sum_{j=1}^{K} \sum_{\ell=0}^{L_j-1} g_{m,\ell}^{(j)} s_j(t - \ell T_c - \tau_j) + \mathrm{i}_m(t) + \mathrm{w}_m(t) \tag{6}$$

where $\mathrm{w}_m(t)$ is additive complex white Gaussian noise with zero mean and variance $\mathrm{E}\{|\mathrm{w}_m(t)|^2\} = \mathcal{N}_o$. The noises $\mathrm{w}_m(t)$ at different antennas are assumed to be mutually independent, i.e., $\mathrm{E}\{\mathrm{w}_m(t_1)\mathrm{w}_{m'}^*(t_2)\} = \mathcal{N}_o \delta[m - m'] \delta(t_1 - t_2)$, where the superscript "$*$" denotes the complex conjugation and $\delta[m]$ is the Kronecker delta function.

III. Space–Time MSINR-SRAKE Receiver for DS-UWB Systems

As shown in Fig. 1, the proposed space–time MSINR-SRAKE receiver comprises M demodulators, Q spatial combiners, and a temporal combiner provided that synchronization and channel estimation are perfect. Each demodulator has Q correlators (i.e., fingers), with each despreading the desired

[1]Assume that the channel delay spread is T_d for all of the channels from each user to each antenna. For the jth user, if the channel to antenna m has an arrival time $(\tau_j + T_m^{(j)})$, then the number of resolvable paths L_j of $h_m^{(j)}(t)$ for $1 \le m \le M$ is approximately $L_j \approx (T_2 - T_1)/T_c$, where $T_1 = \min_{1 \le m \le M}\{\tau_j + T_m^{(j)}\}$ and $T_2 = \max_{1 \le m \le M}\{\tau_j + T_m^{(j)} + T_d\}$ [4], [5].

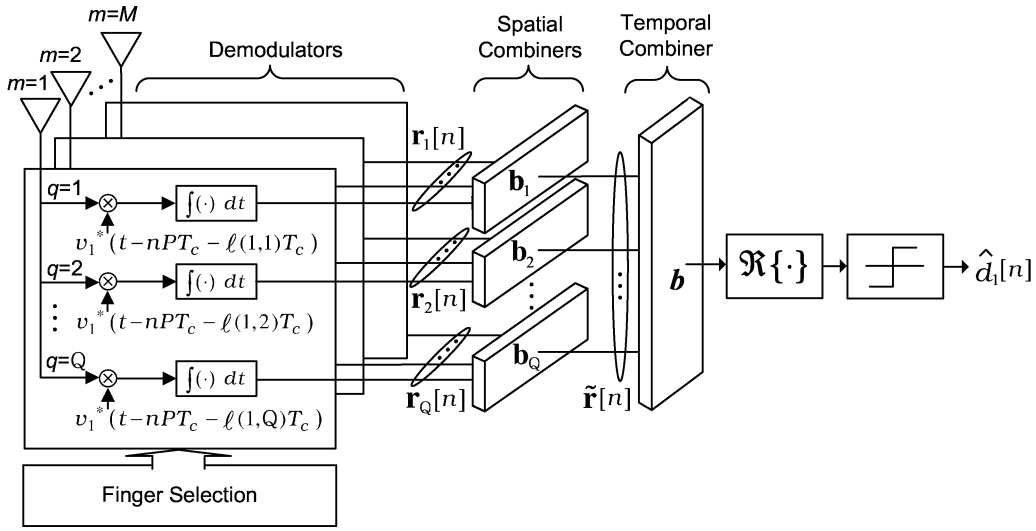

Fig. 1. Proposed space–time MSINR-SRAKE receiver.

signal component from a specific resolvable path according to the FSS used. Both the spatial and temporal MSINR combiners are designed with training signals for effectively suppressing interfering signals and meanwhile achieving diversity gain.

A. Demodulators

For ease of later use, let us define the following notations:

$$\begin{aligned}
&\ell(m,q)\text{: path no. selected for the } q\text{th correlator at antenna } m\\
&C_j = \frac{E_j}{(PT_c)} \quad \text{(average power of user } j)\\
&L_r = P + L_1 - 1
\end{aligned}$$

$$\mathrm{y}_m[i] = \int_{-\infty}^{\infty} y_m(\tau)\psi^*(\tau - iT_c)d\tau \tag{7}$$

$$\mathbf{c}_{m,q} = \left[\underbrace{0,\ldots,0}_{\ell(m,q)}, c_1[0],\ldots,c_1[P-1], \underbrace{0,\ldots,0}_{L_r-P-\ell(m,q)}\right]^{\mathrm{T}} \tag{8}$$

$$\mathbf{y}_m[n] = [\mathrm{y}_m[nP],\ldots,\mathrm{y}_m[nP+L_r-1]]^{\mathrm{T}}. \tag{9}$$

Without loss of generality, we assume that user 1, $s_1(t)$, is the desired user and is perfectly synchronized by the receiver (i.e., $\tau_1 = 0$). The qth correlator output of antenna m during the nth symbol is obtained by

$$\mathrm{r}_{m,q}[n] = \int_{-\infty}^{\infty} y_m(\tau)v_1^*(\tau - nPT_c - \ell(m,q)T_c)\,d\tau \tag{10}$$

where $\ell(m,q) \in \{0,1,\ldots,L_1-1\}$, $q = 1,2,\ldots,Q$, and $m = 1,2,\ldots,M$. By substituting (2) into (10), $\mathrm{r}_{m,q}[n]$ can be further expressed as

$$\mathrm{r}_{m,q}[n] = \sum_{i=0}^{P-1} c_1[i]\mathrm{y}_m[nP + \ell(m,q) + i] = \mathbf{c}_{m,q}^{\mathrm{T}}\mathbf{y}_m[n] \tag{11}$$

where superscript "T" denotes the matrix transpose. Note that the $\mathbf{c}_{m,q}$ in (8) and (11) is a function of $\ell(m,q)$. Moreover, $\mathbf{y}_m[n]$ can be shown, in Appendix I, to be

$$\begin{aligned}
\mathbf{y}_m[n] =& \sqrt{E_1}\mathbf{C}_0^{(1)}\mathbf{g}_m^{(1)}d_1[n] + \underbrace{\sqrt{E_1}\sum_{k\neq n}\mathbf{C}_{n-k}^{(1)}\mathbf{g}_m^{(1)}d_1[k]}_{\text{ISI}}\\
&+ \underbrace{\sum_{j=2}^{K}\sqrt{E_j}\sum_{k=-\infty}^{\infty}\mathbf{C}_{n-k}^{(j)}\mathbf{g}_m^{(j)}d_j[k]}_{\text{MAI}}\\
&+ \underbrace{\sqrt{J}a_m\mathbf{j}[n]}_{\text{NBI}} + \mathbf{w}_m[n]
\end{aligned} \tag{12}$$

which consists of the signal due to the desired DS-UWB symbol $d_1[n]$, the intersymbol interference (ISI), the MAI, the NBI, and the noise, and $\mathbf{g}_m^{(j)}$, $\mathbf{C}_{n-k}^{(j)}$, $\mathbf{j}[n]$, and $\mathbf{w}_m[n]$ are given by (A5), (A8), (A6), and (A7), respectively, in Appendix I.

B. Spatial Combiners

By (11) and (12), one can easily obtain the $M\times 1$ input vector $\mathbf{r}_q[n]$ of the qth spatial combiner (see Fig. 1) as follows:

$$\begin{aligned}
\mathbf{r}_q[n] &= [\mathrm{r}_{1,q}[n], \mathrm{r}_{2,q}[n],\ldots,\mathrm{r}_{M,q}[n]]^{\mathrm{T}}\\
&= \sqrt{E_1}\mathbf{h}_q^{(1)}d_1[n] + \sqrt{E_1}\sum_{k\neq n}\widetilde{\mathbf{h}}_q^{(1)}[n-k]d_1[k]\\
&\quad + \sum_{j=2}^{K}\sqrt{E_j}\sum_{k=-\infty}^{\infty}\widetilde{\mathbf{h}}_q^{(j)}[n-k]d_j[k]\\
&\quad + \sqrt{J}\mathbf{A}_q\mathbf{j}[n] + \widetilde{\mathbf{w}}_q[n]
\end{aligned} \tag{13}$$

where

$$\mathbf{h}_q^{(1)} = \left[\mathbf{c}_{1,q}^{\mathrm{T}}\mathbf{C}_0^{(1)}\mathbf{g}_1^{(1)},\ldots,\mathbf{c}_{M,q}^{\mathrm{T}}\mathbf{C}_0^{(1)}\mathbf{g}_M^{(1)}\right]^{\mathrm{T}} \tag{14}$$

$$\widetilde{\mathbf{h}}_q^{(j)}[n-k] = \left[\mathbf{c}_{1,q}^{\mathrm{T}}\mathbf{C}_{n-k}^{(j)}\mathbf{g}_1^{(j)},\ldots,\mathbf{c}_{M,q}^{\mathrm{T}}\mathbf{C}_{n-k}^{(j)}\mathbf{g}_M^{(j)}\right]^{\mathrm{T}} \tag{15}$$

$$\mathbf{A}_q = [a_1\mathbf{c}_{1,q}, a_2\mathbf{c}_{2,q},\ldots,a_M\mathbf{c}_{M,q}]^{\mathrm{T}} \tag{16}$$

$$\tilde{\mathbf{w}}_q[n]=\left[\mathbf{c}_{1,q}^{\mathrm{T}}\mathbf{w}_1[n],\ldots,\mathbf{c}_{M,q}^{\mathrm{T}}\mathbf{w}_M[n]\right]^{\mathrm{T}}. \tag{17}$$

Let $\mathbf{b}_q$ be the qth spatial combining weight vector (an $M\times 1$ column vector), and then the combiner output $\tilde{\mathrm{r}}_q[n]$ is given by

$$\tilde{\mathrm{r}}_q[n]=\mathbf{b}_q^{\mathrm{H}}\mathbf{r}_q[n] \tag{18}$$

where superscript "H" denotes the matrix conjugate transpose. The SINR of $\tilde{\mathrm{r}}_q[n]$ can be easily shown, from (13) and (18), to be

$$\mathrm{SINR}_o(q)=\frac{E_1\left|\mathbf{b}_q^{\mathrm{H}}\mathbf{h}_q^{(1)}\right|^2}{\mathbf{b}_q^{\mathrm{H}}\mathbf{R}_q\mathbf{b}_q} \tag{19}$$

where

$$\mathbf{R}_q=\mathrm{E}\left\{\left(\mathbf{r}_q[n]-\sqrt{E_1}\mathbf{h}_q^{(1)}d_1[n]\right)\times\left(\mathbf{r}_q[n]-\sqrt{E_1}\mathbf{h}_q^{(1)}d_1[n]\right)^{\mathrm{H}}\right\} \tag{20}$$

is the $M\times M$ interference-plus-noise correlation matrix. Then, one can obtain the optimum spatial MSINR combining weight vector $\mathbf{b}_q$ by maximizing the $\mathrm{SINR}_o(q)$ given by (19) [14]. As a result, the optimum spatial combiner and the associated maximum SINR can be shown to be

$$\mathbf{b}_q=\sqrt{E_1}\mathbf{R}_q^{-1}\mathbf{h}_q^{(1)} \tag{21}$$

and

$$\mathrm{SINR}_o(q)=E_1\left(\mathbf{h}_q^{(1)}\right)^{\mathrm{H}}\mathbf{R}_q^{-1}\mathbf{h}_q^{(1)} \tag{22}$$

respectively. Note that both $\sqrt{E_1}\mathbf{h}_q^{(1)}=\mathrm{E}\{\mathbf{r}_q[n]d_1^*[n]\}$ and $\mathbf{R}_q$ in (20) can be estimated by a sample average of training signals.

C. Temporal Combiner

By stacking all of the $\tilde{\mathrm{r}}_q[n]$ given by (18) as a $Q\times 1$ vector given by

$$\tilde{\mathbf{r}}[n]=[\tilde{\mathrm{r}}_1[n],\tilde{\mathrm{r}}_2[n],\ldots,\tilde{\mathrm{r}}_Q[n]]^{\mathrm{T}} \tag{23}$$

through the same procedure as obtaining the preceding spatial combiners, the optimum temporal combiner $\boldsymbol{b}$ (as shown in Fig. 1) in the maximum output SINR sense can be shown to be

$$\boldsymbol{b}=\boldsymbol{R}^{-1}\boldsymbol{h} \tag{24}$$

where $\boldsymbol{h}=\mathrm{E}\{\tilde{\mathbf{r}}[n]d_1^*[n]\}$ and $\boldsymbol{R}=\mathrm{E}\{(\tilde{\mathbf{r}}[n]-\boldsymbol{h}d_1[n])(\tilde{\mathbf{r}}[n]-\boldsymbol{h}d_1[n])^{\mathrm{H}}\}$ can also be estimated during the training phase. Meanwhile, the SINR of the optimum temporal combiner output $\boldsymbol{b}^{\mathrm{H}}\tilde{\mathbf{r}}[n]$ is given by

$$\mathrm{SINR}_o=\boldsymbol{h}^{\mathrm{H}}\boldsymbol{R}^{-1}\boldsymbol{h}. \tag{25}$$

D. Performance Analysis in the Presence of NBI

By focusing on the impact of NBI upon the receiver performance, let us consider the case of only a single UWB user ($K=1$, thus no MAI), with the following assumptions.

1) The desired DS-UWB signal $s_1(t)$, the NBI $\mathrm{i}_m(t)$, and the noise $\mathrm{w}_m(t)$ are mutually uncorrelated for $m=1,2,\ldots,M$.
2) The channel length L is not a multiple of $(P+1)$, i.e., $L\neq(P+1)k$ for $k\in\mathbb{N}$.
3) The pulse autocorrelation function $R_\psi^{(1)}[i]$ given by (A2) is $R_\psi^{(1)}[i]=\delta[i]$.
4) The spreading sequence $c_1[i]$ has a perfect autocorrelation property, i.e., the autocorrelation sequence of $c_1[i]$ satisfies

$$\mathbf{c}_{m,q}^{\mathrm{T}}\mathbf{c}_{m',q'}=\begin{cases}1, & \text{if } \ell(m,q)=\ell(m',q')\\ 0, & \text{otherwise}\end{cases}. \tag{26}$$

Assumptions 2)–4) imply that the correlations among components of the noise $\mathbf{w}_m[n]$ [by (A4) and (A7)], the ISI and the self-interference[2] in (12) can be ignored. Nevertheless, these assumptions are meritorious since the NBI usually has a much larger power than that of the interference ignored, while the receiver performance analysis due to NBI becomes feasible under these assumptions.

Under the four assumptions above, $\mathbf{h}_q^{(1)}$ given by (14) and $\mathbf{R}_q$ given by (20) can be rewritten as

$$\mathbf{h}_q^{(1)}=\left[g_{1,\ell(1,q)}^{(1)},g_{2,\ell(2,q)}^{(1)},\ldots,g_{M,\ell(M,q)}^{(1)}\right]^{\mathrm{T}} \tag{27}$$

$$\mathbf{R}_q=J\mathbf{A}_q\mathbf{R}_{\mathrm{NBI}}\mathbf{A}_q^{\mathrm{H}}+\mathcal{N}_o\mathbf{I} \tag{28}$$

respectively, where $\mathbf{I}$ is an $M\times M$ identity matrix and

$$\mathbf{R}_{\mathrm{NBI}}=\mathrm{E}\left\{\mathbf{j}[n]\mathbf{j}^{\mathrm{H}}[n]\right\} \tag{29}$$

is the $L_r\times L_r$ correlation matrix of NBI. Then, by substituting (27) and (28) into (22), one can obtain

$$\mathrm{SINR}_o(q)=E_1\left(\mathbf{h}_q^{(1)}\right)^{\mathrm{H}}\left(J\mathbf{A}_q\mathbf{R}_{\mathrm{NBI}}\mathbf{A}_q^{\mathrm{H}}+\mathcal{N}_o\mathbf{I}\right)^{-1}\mathbf{h}_q^{(1)}. \tag{30}$$

In order to investigate how the output SINR depends on NBI, let us define α as the ratio of NBI's bandwidth to the UWB signal's bandwidth and β as the ratio of the carrier frequency

[2]The self-interference consists of the interference induced by correlations of adjacent pulses and interpath interference due to multipath channels.

offset between NBI and the UWB signal to half of the UWB signal's bandwidth as follows:

$$\alpha = \frac{B}{\left(\frac{1}{T_c}\right)} = BT_c \tag{31}$$

$$\beta = \frac{f_o}{\left(\frac{1}{2T_c}\right)} = 2f_oT_c \tag{32}$$

and the pulse $\psi(t)$ is assumed to be the inverse Fourier transform of a raised cosine waveform [16] with unity energy

$$\psi(t) = \frac{\operatorname{sinc}\left(\frac{t}{T_c}\right)}{\sqrt{E_{T_c}}} \frac{\cos\left(\pi\rho\left(\frac{t}{T_c}\right)\right)}{1-4\rho^2\left(\frac{t}{T_c}\right)^2} \tag{33}$$

where $0 \le \rho \le 1$ denotes the rolloff factor of $\psi(t)$ and E_{T_c} is the scaling factor such that $\int |\psi(t)|^2 dt = 1$. As will be proven in Appendix II, the correlation matrix of NBI $\mathbf{R}_{\mathrm{NBI}}$ can be approximated as

$$\mathbf{R}_{\mathrm{NBI}} \approx \frac{1}{E_\alpha B}\left|\Psi_\alpha\left(\frac{\beta}{2\alpha}\right)\right|^2 \widetilde{\mathbf{R}}_{\mathrm{NBI}}(\alpha,\beta) \tag{34}$$

where

$$\Psi_\alpha(f) = \begin{cases} \alpha, & 0 \le |f| < \frac{1-\rho}{2\alpha}, \\ \frac{\alpha}{2}\left\{1+\cos\left[\frac{\pi\alpha}{\rho}\left(|f|-\frac{1-\rho}{2\alpha}\right)\right]\right\}, & \frac{1-\rho}{2\alpha} \le |f| < \frac{1+\rho}{2\alpha}, \\ 0, & \text{otherwise} \end{cases} \tag{35}$$

is the Fourier transform of $\psi_\alpha(t)$ given by (A11), E_α is the energy of $\psi_\alpha(t)$, and $\widetilde{\mathbf{R}}_{\mathrm{NBI}}(\alpha,\beta)$ is an NBI-related correlation matrix given by (A13). By substituting (34) into (30), the $\mathrm{SINR}_o(q)$ then can be approximated as

$$\begin{aligned} &\mathrm{SINR}_o(q) \\ &\quad\approx E_1\left(\mathbf{h}_q^{(1)}\right)^{\mathrm{H}} \\ &\qquad\cdot\left(\frac{J}{E_\alpha B}\left|\Psi_\alpha\left(\frac{\beta}{2\alpha}\right)\right|^2 \mathbf{A}_q\widetilde{\mathbf{R}}_{\mathrm{NBI}}(\alpha,\beta)\mathbf{A}_q^{\mathrm{H}} + \mathcal{N}_o\mathbf{I}\right)^{-1}\mathbf{h}_q^{(1)} \\ &\quad= \sum_{k=1}^{r} \frac{\left|\left(\mathbf{h}_q^{(1)}\right)^{\mathrm{H}}\mathbf{v}_{q,k}(\alpha,\beta)\right|^2}{\left(\frac{J}{C_1}\right)\left(\frac{1}{\alpha E_\alpha P}\right)\left|\Psi_\alpha\left(\frac{\beta}{2\alpha}\right)\right|^2\lambda_{q,k}(\alpha,\beta)+\left(\frac{\mathcal{N}_o}{E_1}\right)} \\ &\qquad+\frac{E_1}{\mathcal{N}_o}\sum_{k=r+1}^{M}\left|\left(\mathbf{h}_q^{(1)}\right)^{\mathrm{H}}\mathbf{v}_{q,k}(\alpha,\beta)\right|^2 \end{aligned} \tag{36}$$

where

$$r = \operatorname{rank}\left(\mathbf{A}_q\widetilde{\mathbf{R}}_{\mathrm{NBI}}(\alpha,\beta)\mathbf{A}_q^{\mathrm{H}}\right). \tag{37}$$

$\{\lambda_{q,k}(\alpha,\beta)\}_{k=1}^{M}$ are the eigenvalues of $\mathbf{A}_q\widetilde{\mathbf{R}}_{\mathrm{NBI}}(\alpha,\beta)\mathbf{A}_q^{\mathrm{H}}$ (with $\lambda_{q,k}(\alpha,\beta) > 0$ for $1 \le k \le r$, and $\lambda_{q,k}(\alpha,\beta) = 0$ for $r+1 \le k \le M$), and $\{\mathbf{v}_{q,k}(\alpha,\beta)\}_{k=1}^{M}$ are the associated eigenvectors.

One can observe, from (36), that the value of $\mathrm{SINR}_o(q)$ is dependent upon NBI-related parameters J/C_1, α, and β, and, more importantly, upon the FSS used, because all of $\mathbf{h}_q^{(1)}$, $\mathbf{A}_q$, $\{\lambda_{q,k}(\alpha,\beta)\}$, and $\{\mathbf{v}_{q,k}(\alpha,\beta)\}$ are functions of the selected $\{\{\ell(m,q)\}_{q=1}^{Q}\}_{m=1}^{M}$. Next, we present four FSSs for the proposed space–time SRAKE receiver and assess their performance based on the $\mathrm{SINR}_o(q)$ approximation, as given by (36).

IV. FSSs for Space-time MSINR-SRAKE Receiver

A. Optimum FSS

The FSS concerns the decision of $\ell(m,q)$ for all $1 \le m \le M$ and $1 \le q \le Q$ to achieve the optimal tradeoff of the receiver performance and complexity (in terms of Q and M). Therefore, the optimum FSS, denoted as the Opt-FSS, is the one that determines $\{\{\ell(m,q)\}_{q=1}^{Q}\}_{m=1}^{M}$ such that the SINR_o given by (25) is maximum for fixed Q and M. However, SINR_o is almost an untractable function of $\{\{\ell(m,q)\}_{q=1}^{Q}\}_{m=1}^{M}$, and thus the optimum $\{\{\ell(m,q)\}_{q=1}^{Q}\}_{m=1}^{M}$ can only be obtained through exhaustive search over $\binom{L_1}{Q}^M$ possible combinations. For instance, for $M=3$, $Q=5$, and $L_1=50$ in UWB multipath channels, around 9.51×10^{18} trials are required, implying that the Opt-FSS is not very practical due to extraordinary computational load. Next, two feasible FSSs (EB-FSS and CEB-FSS) are presented.

B. Energy-Based FSS

For the EB-FSS, $\{\{\ell(m,q)\}_{q=1}^{Q}\}_{m=1}^{M}$ are the set of path numbers such that maximum energy of the desired UWB signal for fixed Q and M can be collected. It is easy to see that

$$\{\ell(m,q)\}^{(\mathrm{EB})} = \arg\max_{\{\ell(m,q)\}}\left\{\sum_{m=1}^{M}\sum_{q=1}^{Q}\left|g_{m,\ell(m,q)}^{(1)}\right|^2\right\} \tag{38}$$

and $|g_{m,\ell(m,q)}^{(1)}| > |g_{m,\ell(m,q+1)}^{(1)}|$ for all $1 \le q \le Q$ and $1 \le m \le M$. Namely, the Q strongest paths out of the L_1 paths of the channel $h_m^{(1)}(t)$ are selected in decreasing order of path gain magnitudes by the demodulator associated with antenna m. A simple example for the EB-FSS is illustrated in Fig. 2 (solid line) for $M=2$, $Q=2$, where the fourth path ($\ell(1,1)=3$) and the sixth path ($\ell(1,2)=5$) of $h_1^{(1)}(t)$, and the third path ($\ell(2,1)=2$) and the eighth path ($\ell(2,2)=7$) of $h_2^{(1)}(t)$ are selected because they are the two strongest paths at each of the two receive antennas, respectively.

According to (36), two observations about the EB-FSS used by the proposed space-time MSINR-SRAKE receiver are given as follows.

1) Because $\mathrm{SINR}_o(q) \to (E_1/\mathcal{N}_o)\|\mathbf{h}_q^{(1)}\|^2$ as $J/C_1 \to 0$, the SINR_o given by (25) can be seen to be

$$\mathrm{SINR}_o \to \frac{E_1}{\mathcal{N}_o}\sum_{m=1}^{M}\sum_{q=1}^{Q}\left|g_{m,\ell(m,q)}^{(1)}\right|^2 \text{ as } \frac{J}{C_1} \to 0 \tag{39}$$

which means that the proposed space–time receiver using the EB-FSS achieves the maximum output SINR of the

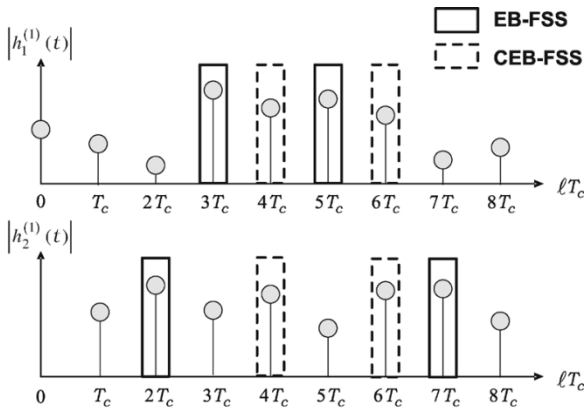

ℓ	0	1	2	3	4	5	6	7	8
$\left\|g_{1,\ell}^{(1)}\right\|$	0.33	0.29	0.06	0.53	0.49	0.51	0.47	0.12	0.23
$\left\|g_{2,\ell}^{(1)}\right\|$	0	0.38	0.55	0.4	0.5	0.27	0.51	0.52	0.31
$\sum_{m=1}^{2}\left\|g_{m,\ell}^{(1)}\right\|^2$	0.33	0.2285	0.3061	0.4409	0.4901	0.333	0.481	0.2848	0.149

Fig. 2. Example illustrating the paths selected by the EB-FSS (solid line) and by the CEB-FSS (dashed line) for $M = 2$ and $Q = 2$.

temporal combiner in the interference-free environment [see (38)].

2) Typically, $\{\ell(m,q)\}^{(\mathrm{EB})} \neq \{\ell(m',q)\}^{(\mathrm{EB})}$ for $m \neq m'$ (i.e., different arrival times associated with the qth strongest path at antennas m and m'). Thus, the two column vectors $\mathbf{c}_{m,q}$ and $\mathbf{c}_{m',q}$ for $m \neq m'$ are linearly independent by (8), thereby leading to $\mathrm{rank}(\mathbf{A}_q) = M$. On the other hand, $\mathrm{rank}(\mathbf{A}_q\widetilde{\mathbf{R}}_{\mathrm{NBI}}(\alpha,\beta)\mathbf{A}_q^{\mathrm{H}}) = M$ in general.[3] Hence, $\mathrm{SINR}_o(q)$ given by (36) can be expressed as

$$\mathrm{SINR}_o(q) \approx \sum_{k=1}^{M} \frac{\left|\left(\mathbf{h}_q^{(1)}\right)^{\mathrm{H}}\mathbf{v}_{q,k}(\alpha,\beta)\right|^2}{\left(\frac{J}{C_1}\right)\left(\frac{1}{\alpha E_\alpha P}\right)\left|\Psi_\alpha\left(\frac{\beta}{2\alpha}\right)\right|^2\lambda_{q,k}(\alpha,\beta)+\left(\frac{\mathcal{N}_o}{E_1}\right)}. \tag{40}$$

Thus, $\mathrm{SINR}_o(q) \to 0$ as $J/C_1 \to \infty$, indicating that the receiver performance will unlimitedly degrade as J/C_1 unlimitedly increases (i.e., not near–far resistent to NBI [19]). Through (40), the receiver performance is relevant to $\{\mathbf{v}_{q,k}(\alpha,\beta)\}$, $\{\lambda_{q,k}(\alpha,\beta)\}$, E_α, and $\Psi_\alpha(\beta/2\alpha)$, all depending on α and β, and the channel $\mathbf{h}_q^{(1)}$ associated with the EB-FSS used. Moreover, due to mixing influence of $\{\mathbf{v}_{q,k}(\alpha,\beta)\}$ and $\mathbf{h}_q^{(1)}$ upon the receiver performance, it is not very tractable to analyze how $\{\mathbf{v}_{q,k}(\alpha,\beta)\}$ affects the receiver performance due to different values of α and β. Nevertheless, the effect of $\{\lambda_{q,k}(\alpha,\beta)\}$, E_α and $\Psi_\alpha(\beta/2\alpha)$ [in the denominator of the term inside the summation of (40)] on the receiver performance with different α and β can be investigated analytically.

Substituting (35) into (40) gives rise to (41), shown at the bottom of this page. In spite of the dependence of $\mathrm{SINR}_o(q)$ on the two parameters α and β according to (41), it is still not trivial to infer the detailed dependence because the channel $\mathbf{h}_q^{(1)}$ is also involved. Next, let us present a "semi-analytical" approach (analytic approach aided with partial simulation) to further investigate how $\mathrm{SINR}_o(q)$ is dependent on α and β, respectively.

A set of 500 realizations of $\{h_m^{(1)}(t)\}_{m=1}^M$ given by (3) was generated by channel model 2 (CM2) [20] for $M = 4$. For each $\{h_m^{(1)}(t)\}_{m=1}^M$, we obtained $\mathbf{A}_q$ and $\mathbf{h}_q^{(1)}$ associated with the EB-FSS for $Q = 1$, $a_m = 1$ for all m, and $c_1[i]$ being a Gold code with $P = 31$, and then obtained $\{(\alpha/E_\alpha)\lambda_{q,k}(\alpha,\beta)\}_{k=1}^M$ for $\beta = 0.6$, and $\mathrm{SINR}_o(q)$ by (41) for $\rho = 0.5$, $E_1/\mathcal{N}_o = 10$ dB. Then, the average of $\{(\alpha/E_\alpha)\lambda_{q,k}(\alpha,\beta)\}_{k=1}^M$ and that of $\mathrm{SINR}_o(q)$ (for different values of α and J/C_1) over the 500 realizations were calculated and shown in Figs. 3 and 4, respectively. One can see, from Fig. 3, that the number of dominant values of $\{(\alpha/E_\alpha)\lambda_{q,k}(\alpha,\beta)\}_{k=1}^M$ increases as α increases, indicating that, if $0 \leq |\beta| < 1+\rho$, $\mathrm{SINR}_o(q)$ given by (41) decreases when α increases, as observed from Fig. 4. Fig. 4 also shows that the performance loss is higher as J/C_1 is larger.

Through the same procedure used to obtain the results shown in Figs. 3 and 4, Fig. 5 shows $\mathrm{SINR}_o(q)$ versus β for $\alpha = 0.05$. One can see, from this figure, that the $\mathrm{SINR}_o(q)$ degrades as

[3]Since $M < L_r$, either of the following two conditions results in $\mathrm{rank}(\mathbf{A}_q\widetilde{\mathbf{R}}_{\mathrm{NBI}}(\alpha,\beta)\mathbf{A}_q^{\mathrm{H}}) \neq M$:

1) $\mathbf{c}_{m,q} \in \mathcal{N}\{\widetilde{\mathbf{R}}_{\mathrm{NBI}}(\alpha,\beta)\}$ for some $m \in \{0,1,\ldots,M\}$, where $\mathcal{N}\{\cdot\}$ denotes the null space, or

2) $\mathbf{c}_{m,q} \notin \mathcal{N}\{\widetilde{\mathbf{R}}_{\mathrm{NBI}}(\alpha,\beta)\}$ for all $1 \leq m \leq M$, but $\exists\ i \neq j, 1 \leq i, j \leq M$, such that $\mathbf{c}_{i,q}^{\mathrm{H}}\bar{\mathbf{v}}_1/\mathbf{c}_{j,q}^{\mathrm{H}}\bar{\mathbf{v}}_1 = \mathbf{c}_{i,q}^{\mathrm{H}}\bar{\mathbf{v}}_2/\mathbf{c}_{j,q}^{\mathrm{H}}\bar{\mathbf{v}}_2 = \cdots = \mathbf{c}_{i,q}^{\mathrm{H}}\bar{\mathbf{v}}_\kappa/\mathbf{c}_{j,q}^{\mathrm{H}}\bar{\mathbf{v}}_\kappa$, where $\kappa = \mathrm{rank}(\widetilde{\mathbf{R}}_{\mathrm{NBI}}(\alpha,\beta))$ and $\{\bar{\mathbf{v}}_k\}_{k=1}^\kappa$ is a basis of the range space of $\widetilde{\mathbf{R}}_{\mathrm{NBI}}(\alpha,\beta)$.

Since $\mathbf{A}_q$ is dependent upon the FSS used and $\widetilde{\mathbf{R}}_{\mathrm{NBI}}(\alpha,\beta)$ is only dependent upon NBI, it is generally true that $\mathrm{rank}(\mathbf{A}_q\widetilde{\mathbf{R}}_{\mathrm{NBI}}(\alpha,\beta)\mathbf{A}_q^{\mathrm{H}}) = M$.

$$\mathrm{SINR}_o(q) \approx \begin{cases} \sum_{k=1}^{M} \dfrac{\left|\left(\mathbf{h}_q^{(1)}\right)^{\mathrm{H}}\mathbf{v}_{q,k}(\alpha,\beta)\right|^2}{\left(\frac{J}{C_1}\right)\left(\frac{1}{P}\right)\left(\frac{\alpha\lambda_{q,k}(\alpha,\beta)}{E_\alpha}\right)+\left(\frac{\mathcal{N}_o}{E_1}\right)}, & 0 \leq |\beta| < 1-\rho \\ \sum_{k=1}^{M} \dfrac{\left|\left(\mathbf{h}_q^{(1)}\right)^{\mathrm{H}}\mathbf{v}_{q,k}(\alpha,\beta)\right|^2}{\left(\frac{J}{C_1}\right)\left(\frac{1}{4P}\right)\left\{1+\cos\left[\frac{\pi}{2\rho}(|\beta|-(1-\rho))\right]\right\}^2\left(\frac{\alpha\lambda_{q,k}(\alpha,\beta)}{E_\alpha}\right)+\left(\frac{\mathcal{N}_o}{E_1}\right)}, & 1-\rho \leq |\beta| < 1+\rho \\ \left(\dfrac{E_1}{\mathcal{N}_o}\right)\left\|\mathbf{h}_q^{(1)}\right\|^2, & \text{otherwise} \end{cases} \tag{41}$$

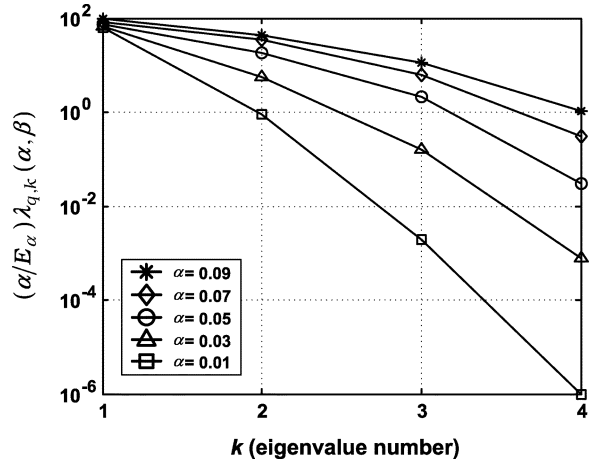

Fig. 3. Semi-analytical results of the averaged $(\alpha/E_\alpha)\lambda_{q,k}(\alpha,\beta)$ over 500 realizations of user 1's channels for $M=4$, $Q=1$, $\rho=0.5$, $\beta=0.6$, and $a_m=1$ for all m, and $c_1[i]$ being a Gold code with $P=31$.

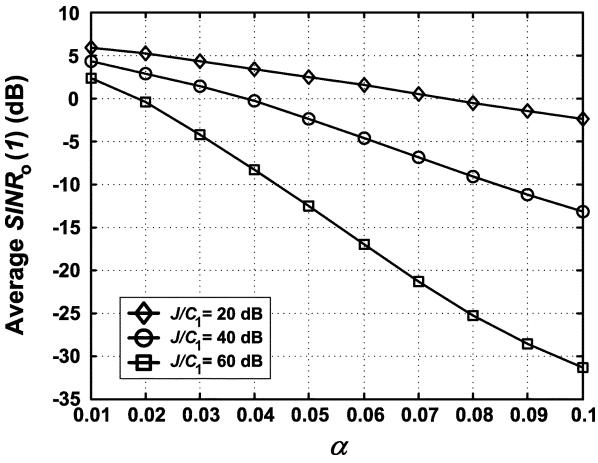

Fig. 4. Semi-analytical results of the averaged $\text{SINR}_o(q)$ approximation over 500 realizations of user 1's channels for $M=4$, $Q=1$, $\rho=0.5$, $E_1/\mathcal{N}_o=10$ dB, $\beta=0.6$, and $a_m=1$ for all m, and $c_1[i]$ being a Gold code with $P=31$.

the NBI approaches the center of the spectrum of UWB signal ($\beta=0$). Furthermore, the degradation becomes more serious as J/C_1 gets larger.

As a result of the preceding analyses, we conclude that the proposed space–time MSINR-SRAKE receiver using the EB-FSS is sensitive to the power ratio (J/C_1), relative bandwidth ratio (α), and relative spectrum location (β) between the NBI and the UWB signal.

C. Constrained Energy-Based FSS

According to observations 1) and 2), the performance of the proposed space–time MSINR-SRAKE receiver using the EB-FSS is sensitive to the strong NBI owing to $r=M$ in general. Therefore, the value of r is the major factor that dominates the receiver performance as J/C_1 is large. Hence, the performance loss ($\text{SINR}_o(q)$) due to larger J/C_1 can be

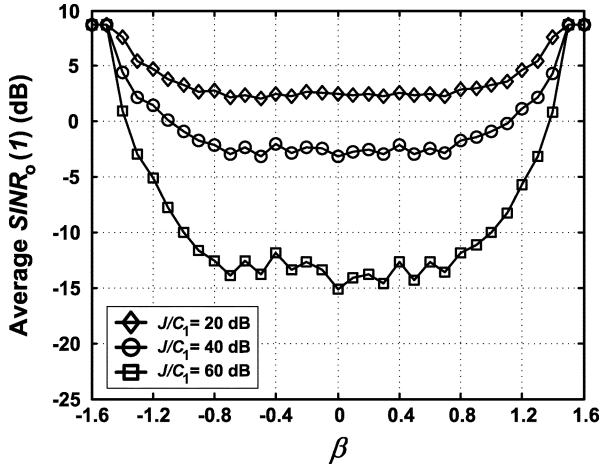

Fig. 5. Semi-analytical results of the averaged $\text{SINR}_o(q)$ approximation over 500 realizations of user 1's channels for $M=4$, $Q=1$, $\rho=0.5$, $E_1/\mathcal{N}_o=10$ dB, $\alpha=0.05$, $a_m=1$ for all m, and $c_1[i]$ being a Gold code with $P=31$.

minimized by making r as small as possible. The minimum $r=1$ can be achieved by considering the FSS with

$$\{\ell(m,q)\}^{(\text{CEB})}=\arg\max_{\{\ell(m,q)\}}\left\{\sum_{q=1}^{Q}\sum_{m=1}^{M}\left|g^{(1)}_{m,\ell(m,q)}\right|^2\right\},$$
$$\text{subject to}\quad \ell(m,q)=\ell(m',q)=\ell(q)\quad \forall m\neq m',\ 1\le q\le Q. \tag{42}$$

Note that the path constraint in (42) is equivalent to $\mathbf{c}_{m,q}=\mathbf{c}_{m',q}=\mathbf{c}_q, \forall\, m\neq m', 1\le q\le Q$. An example for illustrating the CEB-FSS is also shown in Fig. 2 (dashed line) for $M=2$ and $Q=2$, where $\ell(1,1)=\ell(2,1)=\ell(1)=4$ and $\ell(1,2)=\ell(2,2)=\ell(2)=6$.

For the CEB-FSS, one can easily show that

$$\mathbf{A}_q\widetilde{\mathbf{R}}_{\text{NBI}}(\alpha,\beta)\mathbf{A}_q^{\text{H}}=\mathbf{a}\mathbf{a}^{\text{H}}\left(\mathbf{c}_q^{\text{T}}\widetilde{\mathbf{R}}_{\text{NBI}}(\alpha,\beta)\mathbf{c}_q\right) \tag{43}$$

$$\mathbf{v}_{q,1}(\alpha,\beta)=\frac{\mathbf{a}}{\|\mathbf{a}\|} \tag{44}$$

$$\lambda_{q,1}(\alpha,\beta)=\|\mathbf{a}\|^2\mathbf{c}_q^{\text{T}}\widetilde{\mathbf{R}}_{\text{NBI}}(\alpha,\beta)\mathbf{c}_q \tag{45}$$

where $\mathbf{a}=[a_1,a_2,\ldots,a_M]^{\text{T}}$, and therefore $\{\mathbf{v}_{q,k}(\alpha,\beta)=\widetilde{\mathbf{v}}_k\}_{k=2}^{M}$ is an orthonormal basis for the subspace orthogonal to that spanned by $\mathbf{a}$. Now, we can rewrite the $\text{SINR}_o(q)$ given by (36) as follows:

$$\begin{aligned}&\text{SINR}_o(q)\\ &\approx\frac{\left|\left(\mathbf{h}_q^{(1)}\right)^{\text{H}}\mathbf{v}_{q,1}(\alpha,\beta)\right|^2}{\left(\frac{J}{C_1}\right)\left(\frac{1}{\alpha E_\alpha P}\right)\left|\Psi_\alpha\left(\frac{\beta}{2\alpha}\right)\right|^2\lambda_{q,1}(\alpha,\beta)+\left(\frac{\mathcal{N}_o}{E_1}\right)}\\ &\quad+\frac{E_1}{\mathcal{N}_o}\sum_{k=2}^{M}\left|\left(\mathbf{h}_q^{(1)}\right)^{\text{H}}\mathbf{v}_{q,k}(\alpha,\beta)\right|^2\\ &=\frac{\left|\left(\mathbf{h}_q^{(1)}\right)^{\text{H}}\frac{\mathbf{a}}{\|\mathbf{a}\|}\right|^2}{\left(\frac{J}{C_1}\right)\left(\frac{1}{\alpha E_\alpha P}\right)\left|\Psi_\alpha\left(\frac{\beta}{2\alpha}\right)\right|^2\left(\|\mathbf{a}\|^2\mathbf{c}_q^{\text{T}}\widetilde{\mathbf{R}}_{\text{NBI}}(\alpha,\beta)\mathbf{c}_q\right)+\left(\frac{\mathcal{N}_o}{E_1}\right)}\\ &\quad+\frac{E_1}{\mathcal{N}_o}\sum_{k=2}^{M}\left|\left(\mathbf{h}_q^{(1)}\right)^{\text{H}}\widetilde{\mathbf{v}}_k\right|^2,\quad\text{[by (44) and (45)].}\end{aligned} \tag{46}$$

According to (46), two observations about the CEB-FSS are given as follows.

3) As $J/C_1 \to \infty$,

$$\text{SINR}_o(q) \to \left(\frac{E_1}{\mathcal{N}_o}\right) \sum_{k=2}^{M} \left| \left(\mathbf{h}_q^{(1)}\right)^{\text{H}} \widetilde{\mathbf{v}}_k \right|^2$$

which is not only independent of NBI (characterized by α and β) but also increases as $E_1/\mathcal{N}_o$ is increased. Meanwhile, the effects of α and β on the receiver performance loss is also minimized. Therefore, comparing the $\text{SINR}_o(q)$ given by (46) and that given by (40), the CEB-FSS outperforms the EB-FSS as long as J/C_1 is large enough, and the former is much more robust against the NBI than the latter.

4) Due to the path constraint in (42), the amount of the collected desired UWB signal energy using the CEB-FSS is less than or equal to that using the EB-FSS in general, which means that the receiver performance using the EB-FSS can be better than that using the CEB-FSS, as J/C_1 is not very large.

D. Hybrid Energy-Based FSS

For the proposed space–time receiver, by observations 1)–4), the CEB-FSS is preferred to the EB-FSS when the NBI is the dominant interference (J/C_1 is large); however, the EB-FSS becomes preferable to the CEB-FSS if the NBI is not strong. A judicious combination of the EB-FSS and CEB-FSS is the HEB-FSS, which performs better than both the EB-FSS and CEB-FSS for all levels of J/C_1, α, and β, as follows.

Step 1) Obtain $\{\ell(m,q)\}^{(\text{EB})}$ using (38) and $\{\ell(m,q)\}^{(\text{CEB})}$ using (42), and the associated $\text{SINR}_o^{(\text{EB})}$ and $\text{SINR}_o^{(\text{CEB})}$ using (25).

Step 2) Obtain

$$\{\ell(m,q)\}^{(\text{HEB})} = \begin{cases} \{\ell(m,q)\}^{(\text{EB})}, & \text{SINR}_o^{(\text{EB})} \geq \text{SINR}_o^{(\text{CEB})} \\ \{\ell(m,q)\}^{(\text{CEB})}, & \text{otherwise.} \end{cases} \tag{47}$$

In other words, the proposed HEB-FSS performs like the EB-FSS does for weak NBI and like the CEB-FSS does for strong NBI, while the computational load of the former is the sum of those of the latter two. Let us conclude this section with the following four remarks about the proposed FSSs.

1) The proposed space–time MSINR-SRAKE receiver for DS-UWB systems as well as the presented four FSSs (i.e., Opt-FSS, EB-FSS, CEB-FSS, and HEB-FSS) also apply to other RAKE-based UWB systems such as TH-UWB systems.

2) As for the case of the presence of both MAI and NBI under the assumptions 1)–4) and the assumption that the symbol sequences $d_j[n]$, $j = 1, 2, \ldots, K$, are mutually independent and are independent of NBI $\text{i}_m(t)$ and noise $\text{w}_m(t)$, $\text{SINR}_o(q)$ given by (22) can be proven, as will be shown in Appendix III, to be

$$\text{SINR}_o(q) = \sum_{k=1}^{r} \frac{\left| \left(\mathbf{h}_q^{(1)}\right)^{\text{H}} \mathbf{u}_{q,k} \right|^2}{\left(\frac{J}{C_1}\right)\left(\frac{1}{T_c P}\right)\widetilde{\lambda}_{q,k} + \left(\frac{\mathcal{N}_o}{E_1}\right)} + \frac{E_1}{\mathcal{N}_o} \sum_{k=r+1}^{M} \left| \left(\mathbf{h}_q^{(1)}\right)^{\text{H}} \mathbf{u}_{q,k} \right|^2 \tag{48}$$

where $\{\widetilde{\lambda}_{q,k}\}$ are the eigenvalues of $\widetilde{\mathbf{R}}_{IN}^{-1}\widetilde{\mathbf{R}}_{NB}$ [see (A16) and (A17)], r is the rank of $\widetilde{\mathbf{R}}_{NB}$ [see (A20)], and $\mathbf{u}_{q,k}$ is the kth column of the matrix $\mathbf{U}$ given by (A21). Thus, with observations similar to 1) and 3) for NBI only, we can conclude that, in the presence of both MAI and NBI, the proposed space–time receiver using the CEB-FSS ($r = 1$) can have better multiple access capability than that using the EB-FSS ($r = M$) as J/C_1 is large.

3) The proposed space–time MSINR-SRAKE receiver considers the cascade structure of spatial processing followed by temporal processing. One can also consider the corresponding receiver with the joint structure of simultaneous spatial and temporal processing [14]. Following the same performance analysis as done for the cascade structure, one can show similar analytical results for the joint structure. In other words, as J/C_1 is large, the receiver performance with the CEB-FSS used is better than that with the EB-FSS used, and the HEB-FSS also applies to this structure.

4) Assumptions 1)–4) regarding the omission of the effects of ISI and self-interference induced by pulse overlaps and nonperfect autocorrelation property of spreading sequences seem to limit the value of the above performance analyses. We will show below that these performance analyses are consistent with simulation results because these effects are negligible when compared with the effects of strong NBI.

V. Simulation Results

This section presents some simulation results to justify the efficacy of the proposed space–time MSINR-SRAKE receiver and the proposed FSSs. The baseband DS-UWB signals for the desired user and MAI were generated using (1) and (2), where $c_j[i]$ was a Gold sequence of length 31 ($P = 31$) and the chip duration was $T_c = 0.6$ ns. The pulse waveform $\psi(t)$ was the inverse Fourier transform of the raised cosine function with the rolloff factor $\rho = 0.5$ and Nyquist frequency $1/(2T_c)$ (see (33) and [16]). The 3-dB passband bandwidth of $\psi(t)$ was $1/T_c = 1.67$ GHz, which contains most of the pulse energy, therefore, the UWB signal approximately has passband bandwidth $1/T_c$. The carrier frequency was 4.5 GHz.

If not mentioned specifically, the UWB indoor channel model of CM2 in [20] was used in the simulation, and the channel's coherence time was assumed to be longer than the duration of a data frame of 200 DS-UWB symbols. The NBI was generated by passing a real white Gaussian signal through a band-limited filter (passband bandwidth B) with an offset f_o from the

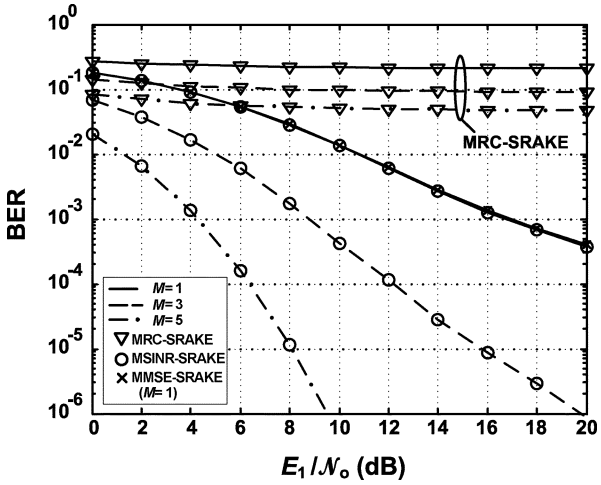

Fig. 6. Performance (BER) of the proposed space–time MSINR-SRAKE receiver and three other SRAKE receivers using the EB-FSS in the presence of only NBI (without MAI) for $B = 40$ MHz, $f_o = 0.5$ GHz, $J/C_1 = 20$ dB, and $Q = 5$.

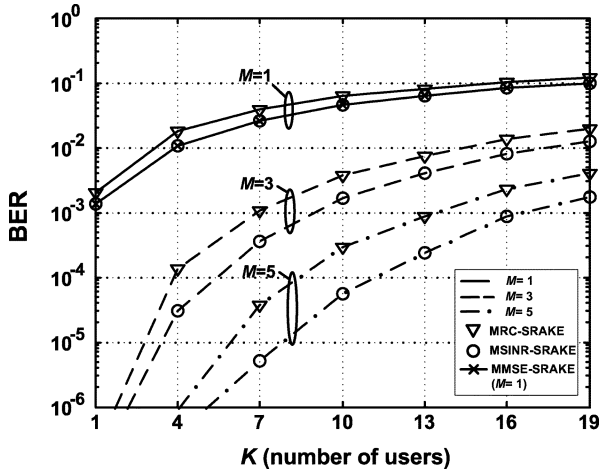

Fig. 7. Performance (BER) of the proposed space–time MSINR-SRAKE receiver and three other SRAKE receivers using the EB-FSS in the presence of only MAI (without NBI) for $E_1/\mathcal{N}_o = 10$ dB, $Q = 5$, and $M = 1, 3$, and 5.

carrier frequency of the UWB signal. The simulation results [in terms of bit error rate (BER)] of the proposed space–time MSINR-SRAKE receiver, the space–time MRC-SRAKE receiver [8], the time-only MRC-SRAKE receiver [5], and the time-only MMSE-SRAKE receiver [7] with a chosen FSS were obtained from 5×10^4 independent frames.

A. Performance of the Proposed Space–Time MSINR-SRAKE Receiver

Fig. 6 displays some simulation results (BERs versus $E_1/\mathcal{N}_o$) of the four receivers using the EB-FSS in the presence of only NBI (without MAI), for $B = 40$ MHz, $f_o = 0.5$ GHz, $J/C_1 = 20$ dB, $Q = 5$, and $M = 1, 3$, and 5. One can observe, from this figure, that the MRC-based receivers are interference-limited even if multiple antennas were used, whereas the MMSE (only for $M = 1$) or MSINR-based receivers perform better for either higher $E_1/\mathcal{N}_o$ or larger M. In particular, in addition to interference mitigation, the increased degrees of freedom by using multiple receive antennas ($M = 5$) provide substantial spatial and path diversity gains for the space–time MSINR-SRAKE receiver.

Fig. 7 displays some simulation results (BERs versus number of users K) of the four receivers using the EB-FSS in the presence of only MAI (without NBI), for near–far ratio equal to 0 dB, $E_1/\mathcal{N}_o = 10$ dB, $Q = 5$, and $M = 1, 3$ and 5. It can be seen, from this figure, that larger multiple-access capacity is attained when multiple receive antennas are used for all four receivers; however, the amount of multiple-access capacity associated with the proposed space–time MSINR-SRAKE receiver is largest.

B. Performance Comparison of the Proposed FSSs

Fig. 8(a) displays some simulation results (BERs versus $E_1/\mathcal{N}_o$) of the proposed space–time MSINR-SRAKE receiver using either the EB-FSS or CEB-FSS in the presence of only NBI (without MAI), for $B = 40$ MHz, $f_o = 0.5$ GHz, $J/C_1 = 40$ dB, $M = 1$ and 2, and $Q = 3$, 5, and 7. It can be seen, from Fig. 8(a), that the receiver performance using the CEB-FSS for $M = 2$ is better than using EB-FAS for $M = 1$ and $M = 2$. Note that the EB-FSS and CEB-FSS are identical for $M = 1$. One can also observe from Fig. 8(a) that the receiver performance using EB-FSS for $M = 2$ is worse than for $M = 1$ for all $Q = 3$, 5, and 7 for this case of $J/C_1 = 40$ dB which seems not very reasonable. To further investigate the insights about this, Fig. 8(b) displays the corresponding results for $Q = 5$, and $J/C_1 = 20$, 30, and 40dB. One can see from Fig. 8(b) that the receiver performance using EB-FSS with $M = 2$ is better (worse) than with $M = 1$ for $J/C_1 = 20$ dB (for $J/C_1 = 40$ dB), and for $J/C_1 = 30$ dB, it is slightly better with $M = 2$ than with $M = 1$ for $E_b/\mathcal{N}_o$ smaller than 10 dB. This indicates that the receiver performance using EB-FSS is susceptible to the value of J/C_1. These results demonstrate that, in the presence of strong NBI ($J/C_1 \geq 30$ dB), the CEB-FSS is a much better choice than the EB-FSS.

Fig. 9 illustrates some simulation results (BERs versus J/C_1) of the proposed space–time MSINR-SRAKE receiver using either the EB-FSS or CEB-FSS in the presence of NBI (without MAI), for $E_1/\mathcal{N}_o = 10$ dB, $M = 3$, $Q = 5$, $\beta = 0.6$ ($f_o = 0.5$ GHz), and $\alpha = 0.012, 0.024, 0.06$, and 0.12 (i.e., $B = 20, 40, 100$, and 200 MHz). From this figure, one can observe that the proposed space—time receiver using the CEB-FSS is quite robust against NBI for different values of (J/C_1) and α. On the other hand, the receiver performance degradation is larger for either higher J/C_1 or larger α when the EB-FSS is used.

Fig. 10 presents some simulation results (BERs versus β) of the proposed space–time receiver using either the EB-FSS or CEB-FSS in the presence of NBI (without MAI), for $E_1/\mathcal{N}_o = 10$ dB, $\alpha = 0.048$ ($B = 80$ MHz), $M = 3$, $Q = 5$, and $J/C_1 = 40$ and 60 dB. One can see from this figure that the proposed space-time receiver using the CEB-FSS is insensitive to the variations of β, however, the receiver performance using the EB-FSS degrades as $|\beta|$ approaches 0. These simulation results are also consistent with observations 2) and 4). Moreover, the simulation results of Figs. 9 and 10 associated with the EB-FSS

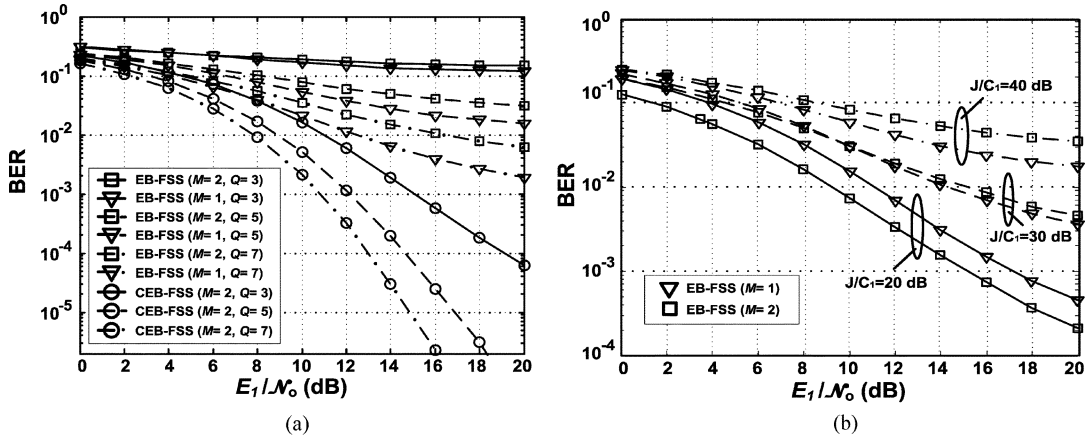

Fig. 8. Performance (BER) of the proposed space–time MSINR-SRAKE receiver using the EB-FSS or CEB-FSS in the presence of only NBI (without MAI) for $M = 1$ and 2, $B = 40$ MHz, $f_o = 0.5$ GHz. (a) $J/C_1 = 40$ dB, and $Q = 3, 5$, and 7. (b) $Q = 5$, and $J/C_1 = 20, 30$, and 40 dB.

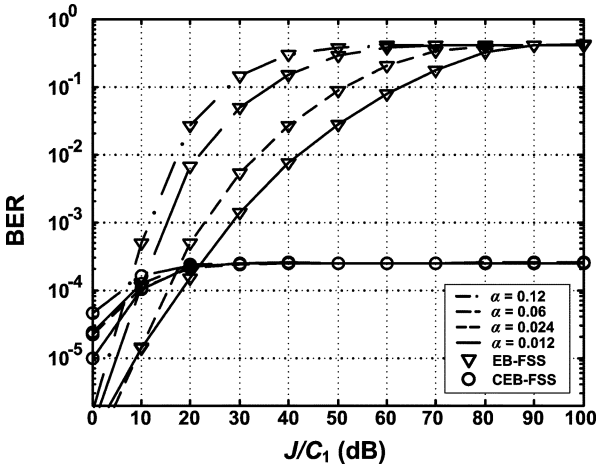

Fig. 9. Performance (BER) of the proposed space–time MSINR-SRAKE receiver using the EB-FSS or CEB-FSS in the presence of only NBI (without MAI) for $E_1/\mathcal{N}_o = 10$ dB, $M = 3$, $Q = 5$, and $\beta = 0.6$ (i.e., $f_o = 0.5$ GHz).

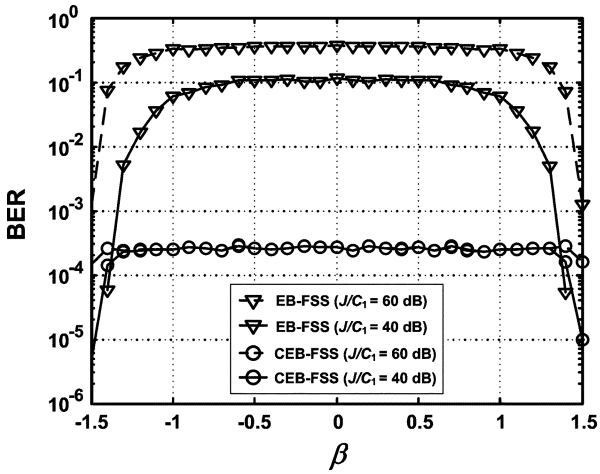

Fig. 10. Performance (BER) of the proposed space–time MSINR-SRAKE receiver using the EB-FSS or CEB-FSS in the presence of only NBI (without MAI) for $E_1/\mathcal{N}_o = 10$ dB, $\alpha = 0.048$ (i.e., $B = 80$ MHz), $M = 3$, and $Q = 5$.

are also consistent with the preceding semi-analytical results (see Figs. 4 and 5) presented in Section IV-B.

Fig. 11 exhibits some simulation results (BERs versus $E_1/\mathcal{N}_o$) of the proposed space–time receiver using either the EB-FSS or CEB-FSS in the presence of only NBI (without MAI), for $B = 40$ MHz, $f_o = 0.5$ GHz, $M = 3$, $Q = 5$, and $J/C_1 = 20$ and 40 dB, under CM1, CM2, CM3, and CM4 UWB channels [20], respectively. One can see from Fig. 11 that the receiver performance using the EB-FSS is interference-limited with an error floor while that using the CEB-FSS is not interference-limited with decreasing BER for larger $E_1/\mathcal{N}_o$. Moreover, the receiver performance using the EB-FSS for $J/C_1 = 40$ dB is much worse than that obtained for $J/C_1 = 20$ dB, whereas that using the CEB-FSS is almost the same for both $J/C_1 = 20$ and 40 dB. The performance differences using the CEB-FSS (with $r = 1$) and the EB-FSS are larger for CM2, CM3, and CM4 than for CM1 since CM1 is a line-of-sight channel with a higher possibility of $r < M = 3$ when the EB-FSS is used. These simulation results are also consistent with observations 2) and 3).

Fig. 12 displays some simulation results (BERs versus K) of the proposed space–time MSINR-SRAKE receiver using either the EB-FSS or CEB-FSS in the presence of both NBI and MAI, for $E_1/\mathcal{N}_o = 10$ dB, $Q = 5$, $M = 4$, $J/C_1 = 40$ dB, $B = 40$ MHz, $f_o = 0.5$ GHz, and near–far ratio equal to 0 dB (i.e., $E_i = E_j$ for all $i \neq j$). One can see, from this figure, that the proposed space–time MSINR-SRAKE receiver using the CEB-FSS can provide better multiple-access capability than that using the EB-FSS when a strong NBI is present. These results also coincide with Remark 2).

Fig. 13 shows some simulation results (BERs versus J/C_1) of the proposed space–time MSINR-SRAKE receiver using the proposed four FSSs in the presence of NBI (without MAI), for $E_1/\mathcal{N}_o = 10$ dB, $B = 80$ MHz, $f_o = 0.5$ GHz, $M = 3$, and $Q = 1$, and the channels are assumed to be independent and identically distributed (i.i.d.) Rayleigh fading channels with $L_1 = 10$ and $\sum_{\ell=1}^{L_1} |g_{m,\ell}^{(1)}|^2 = 1$ for all $1 \leq m \leq M$. One can see that the receiver performance using the HEB-FSS is uniformly better than that using either the EB-FSS or CEB-FSS. However, the receiver performance using the HEB-FSS

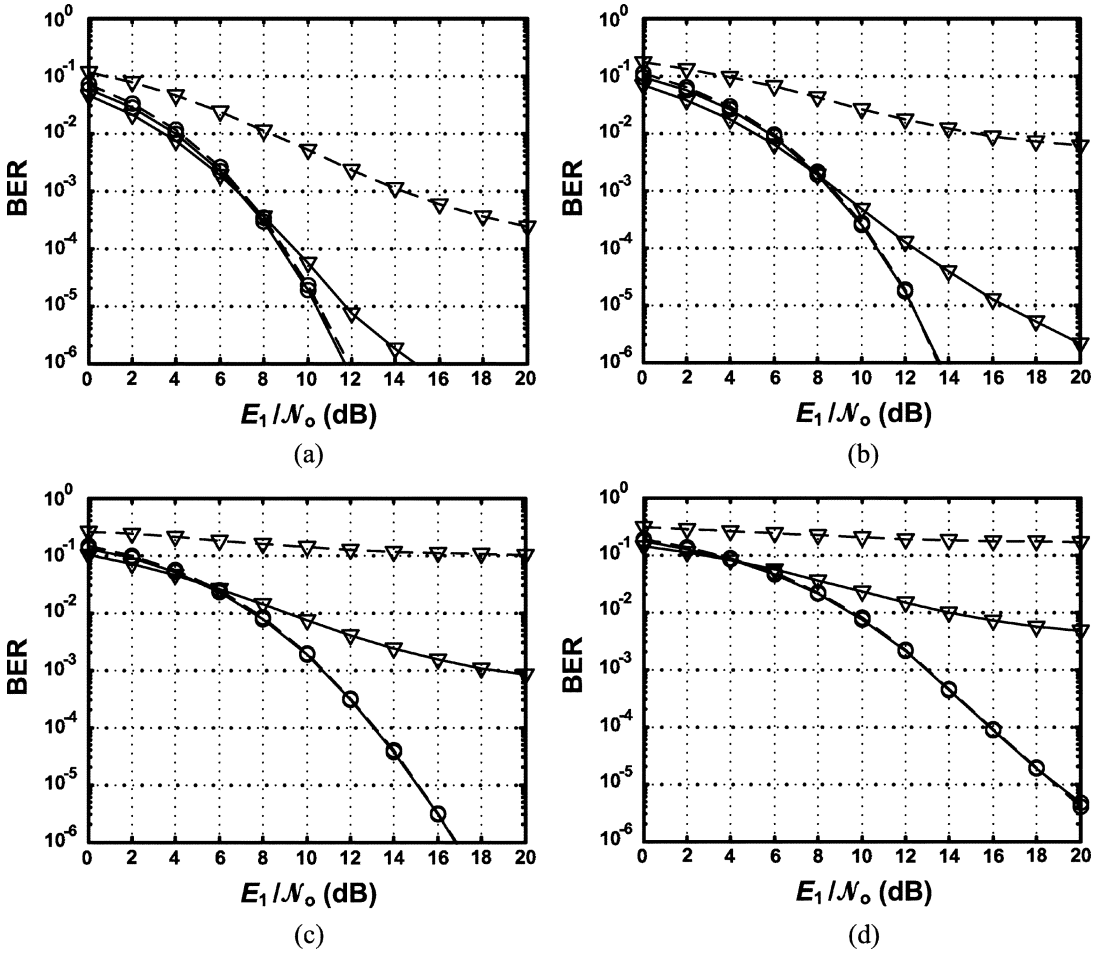

Fig. 11. Performance (BER) of the proposed space–time MSINR-SRAKE receiver using the EB-FSS ($\bigtriangledown$) or CEB-FSS ($\bigcirc$) in the presence of only NBI (without MAI) under UWB channels (a) CM1, (b) CM2, (c) CM3, and (d) CM4 for $B = 40$ MHz, $f_o = 0.5$ GHz, $J/C_1 = 20$ (solid line) and 40 (dashed line) dB, $M = 3$, and $Q = 5$.

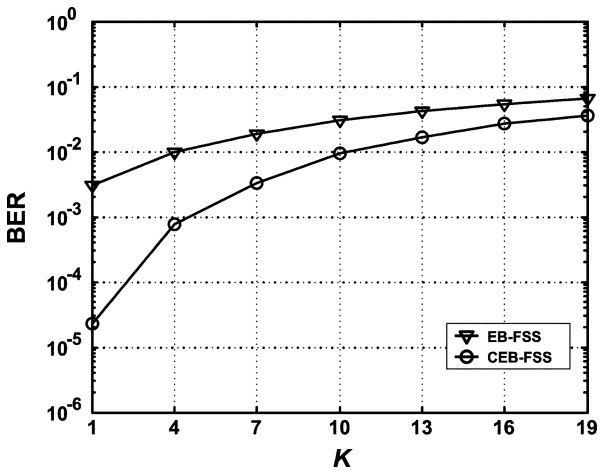

Fig. 12. Performance (BER) of the proposed space–time MSINR-SRAKE receiver using the EB-FSS or CEB-FSS in the presence of both NBI and MAI for $E_1/\mathcal{N}_o = 10$ dB, $J/C_1 = 40$ dB, $B = 40$ MHz, $M = 4$, and $Q = 5$.

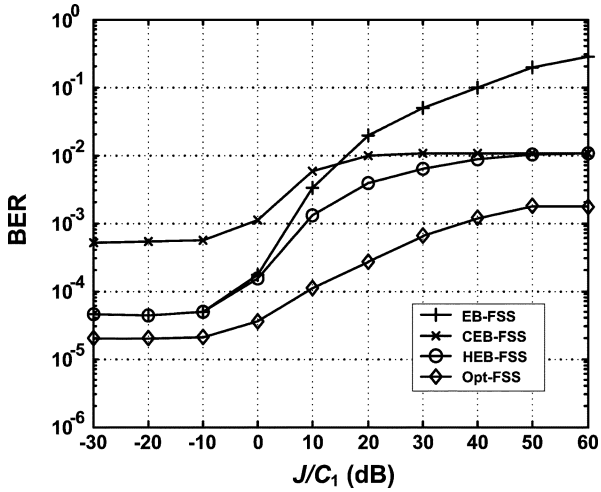

Fig. 13. Performance (BER) of the proposed space–time MSINR-SRAKE receiver using the proposed four FSSs in the presence of only NBI (without MAI) for $E_1/\mathcal{N}_o = 10$ dB, $B = 80$ MHz, $f_o = 0.5$ GHz, $M = 3$, and $Q = 1$.

and that using the Opt-FSS are comparable for both low and high J/C_1, while the computational load for the former is significantly lower than for the latter.

C. Complexity of the Proposed SRAKE Receiver

The above simulation results have justified significant performance improvement of the proposed space–time

MSINR-SRAKE receiver over the MRC-based SRAKE receiver and time-only SRAKE receivers at the expense of computing Q spatial filter $(M \times 1)$ weights and one temporal filter $(Q \times 1)$ weights. The major computational complexity for obtaining the spatial filters and temporal filter resides in the inversion of correlation matrices $\mathbf{R}_q^{-1}$, $q = 1, 2, \ldots, Q$, and $\boldsymbol{R}^{-1}$. There have been many efficient algorithms for obtaining these filter weights without directly computing the matrix inversion [9]. Moreover, Q (which is the number of selected fingers) and M (which is the number of receive antennas) are not very large in general. So the proposed space–time MSINR-SRAKE receiver is practical and feasible.

VI. Conclusion

We have presented a space–time MSINR-SRAKE receiver for DS-UWB systems using multiple antennas in indoor UWB overlay environments (see Fig. 1), for which the selected Q paths at each antenna are determined by the FSS used, and the information data are then estimated through the use of Q spatial combiners and one temporal combiner. An analysis of the receiver performance in the presence of NBI was carried out to show the dependence of receiver performance upon the NBI-related parameters J/C_1, α, and β and upon the FSS used. The analysis concludes that this receiver is robust against NBI when the CEB-FSS is used, and the receiver using the EB-FSS has better performance than that using the CEB-FSS when the NBI is weak. Moreover, the receiver using the HEB-FSS performs better than using either of EB-FSS and CEB-FSS, but its computational load is also the sum of that using the EB-FSS and that using the CEB-FSS. Some simulation results were also presented to demonstrate that the proposed space—time receiver significantly outperforms the existing time-only SRAKE receivers and space—time MRC-SRAKE receivers in terms of NBI suppression and multiple-access capability. Therefore, the proposed space–time MSINR-SRAKE receiver using the HEB-FSS is suited for reliable communications in the UWB overlay environments.

Appendix I
Proof of (12)

Substituting (1) and (6) into (7) yields

$$\mathrm{y}_m[i] = \sum_{j=1}^{K} \sqrt{E_j} \sum_{k=-\infty}^{\infty} d_j[k] \sum_{\ell=0}^{L_j-1} g_{m,\ell}^{(j)} \cdot \sum_{n=0}^{P-1} c_j[n] \cdot R_\psi^{(j)}[i-\ell-n-kP] + \sqrt{J} a_m \mathcal{I}[i] + W_m[i] \tag{A1}$$

where

$$R_\psi^{(j)}[i] = \int_{-\infty}^{\infty} \psi(\tau)\psi^*(\tau - iT_c + \tau_j)d\tau \tag{A2}$$

$$\mathcal{I}[i] = \int_{-\infty}^{\infty} \mathrm{b}(\tau) e^{j2\pi f_o \tau} \psi^*(\tau - iT_c)d\tau \tag{A3}$$

$$W_m[i] = \int_{-\infty}^{\infty} \mathrm{w}_m(\tau)\psi^*(\tau - iT_c)d\tau. \tag{A4}$$

Then, substituting (A1) into (9) gives rise to (12), in which

$$\mathbf{g}_m^{(j)} = \left[g_{m,0}^{(j)}, \ldots, g_{m,L_j-1}^{(j)}\right]^{\mathrm{T}} \tag{A5}$$

$$\mathbf{j}[n] = [\mathcal{I}[nP], \ldots, \mathcal{I}[nP + L_r - 1]]^{\mathrm{T}} \tag{A6}$$

$$\mathbf{w}_m[n] = [W_m[nP], \ldots, W_m[nP + L_r - 1]]^{\mathrm{T}} \tag{A7}$$

and $\mathbf{C}_{n-k}^{(j)}$ is an $L_r \times L_j$ matrix with the (p, q)th entry given by

$$\left[\mathbf{C}_{n-k}^{(j)}\right]_{p,q} = \sum_{i=0}^{P-1} c_j[i] R_\psi^{(j)}\left[(n-k)P - i + p - q\right]. \tag{A8}$$

Appendix II
Proof of (34)

The correlation function of $b(t)$ (i.e., the inverse Fourier transform of $S_b(f)$) can be easily shown to be

$$R_b(\tau) = \mathrm{E}\left\{b(t+\tau)b^*(t)\right\} = \mathrm{sinc}(B\tau). \tag{A9}$$

According to (29), (A3) and (A6), the (p, q)th element of $\mathbf{R}_{\mathrm{NBI}}$ can be expressed as

$$\begin{aligned}
&[\mathbf{R}_{\mathrm{NBI}}]_{p,q} \\
&= \mathrm{E}\left\{\mathcal{I}[nP+p-1]\mathcal{I}^*[nP+q-1]\right\} \\
&= \mathrm{E}\left\{ \int_{-\infty}^{\infty} b\left(t_1 + (nP+p-1)T_c\right) \right. \\
&\qquad \times e^{j2\pi f_o (t_1 + (nP+p-1)T_c)} \psi^*(t_1) dt_1 \\
&\qquad \times \int_{-\infty}^{\infty} b^*\left(t_2 + (nP+q-1)T_c\right) \\
&\qquad \left. \times e^{-j2\pi f_o (t_2 + (nP+q-1)T_c)} \psi(t_2) dt_2 \right\} \\
&= \int_{-\infty}^{\infty}\int_{-\infty}^{\infty} R_b\left(t_1 - t_2 + (p-q)T_c\right) \\
&\qquad \times e^{j2\pi f_o (t_1 - t_2 + (p-q)T_c)} \psi^*(t_1)\psi(t_2) dt_1 dt_2 \\
&= \frac{1}{E_\alpha B} \int_{-\infty}^{\infty}\int_{-\infty}^{\infty} \mathrm{sinc}\left(t_1' - t_2' + (p-q)\alpha\right) \\
&\qquad \times e^{j\pi\left(\frac{\beta}{\alpha}\right)\left(t_1' - t_2' + (p-q)\alpha\right)} \psi_\alpha\left(t_1'\right) \psi_\alpha\left(t_2'\right) dt_1' dt_2'
\end{aligned} \tag{A10}$$

where we have used $R_b(\tau)$ given by (A9), $\alpha = BT_c$ given by (31), and $\beta = 2f_oT_c$ given by (32) and made variable changes of $t_1' = Bt_1$ and $t_2' = Bt_2$ in the derivation of (A10), and

$$\psi_\alpha(t) = \mathrm{sinc}\left(\frac{t}{\alpha}\right) \frac{\cos\left(\pi\rho\left(\frac{t}{\alpha}\right)\right)}{1 - 4\rho^2\left(\frac{t}{\alpha}\right)^2} \tag{A11}$$

is the inverse Fourier transform of a raised cosine function and E_α is the pulse energy of $\psi_\alpha(t)$.

By letting $\Psi_\alpha(f)$ be the Fourier transform of $\psi_\alpha(t)$ and assuming that $\alpha \ll 1$, $[\mathbf{R}_{\rm NBI}]_{p,q}$ in (A10) can be further approximated as follows:

$$\begin{aligned}
&[\mathbf{R}_{\rm NBI}]_{p,q} \\
&= \frac{1}{E_\alpha B} \int_{-\infty}^{\infty} \psi_\alpha(t_1') \int_{-\infty}^{\infty} \operatorname{sinc}(t_1' - t_2' + (p-q)\alpha) \\
&\quad \times e^{j\pi\left(\frac{\beta}{\alpha}\right)(t_1' - t_2' + (p-q)\alpha)} \psi_\alpha(t_2')\, dt_2' dt_1' \\
&\approx \frac{1}{E_\alpha B} \Psi_\alpha\left(\frac{\beta}{2\alpha}\right) \int_{-\infty}^{\infty} \psi_\alpha(t_1') \operatorname{sinc}(t_1' + (p-q)\alpha) \\
&\quad \times e^{j\pi\left(\frac{\beta}{\alpha}\right)(t_1' + (p-q)\alpha)} dt_1' \\
&\approx \frac{1}{E_\alpha B} \left|\Psi_\alpha\left(\frac{\beta}{2\alpha}\right)\right|^2 \operatorname{sinc}((p-q)\alpha)\, e^{j\pi\beta(p-q)}
\end{aligned} \tag{A12}$$

where $\Psi_\alpha(f) S_b(f - (\beta/2\alpha)) \approx \Psi_\alpha(\beta/2\alpha) S_b(f - (\beta/2\alpha))$ (due to the assumption of $\alpha \ll 1$) was used in the derivations of the last two lines of (A12). Finally, let $\widetilde{\mathbf{R}}_{\rm NBI}(\alpha, \beta)$ be a correlation matrix with the (p,q)th element given by

$$\left[\widetilde{\mathbf{R}}_{\rm NBI}(\alpha,\beta)\right]_{p,q} = \operatorname{sinc}((p-q)\alpha)\, e^{j\pi\beta(p-q)}. \tag{A13}$$

By (A12) and (A13), one can obtain $\mathbf{R}_{\rm NBI}$ as given by (34).

Appendix III
Proof of (48)

Under the assumptions 1)–4) and the assumption that the symbol sequences $d_j[n]$, $j = 1, 2, \ldots, K$, are mutually independent and are independent of NBI $\mathrm{i}_m(t)$ and noise $\mathrm{w}_m(t)$, the interference-plus-noise correlation matrix $\mathbf{R}_q$ given by (20) can be easily shown to be

$$\begin{aligned}
\mathbf{R}_q = &\sum_{j=2}^{K} E_j \sum_{k=-\infty}^{\infty} \widetilde{\mathbf{h}}_q^{(j)}[n-k] \left(\widetilde{\mathbf{h}}_q^{(j)}[n-k]\right)^{\rm H} \\
&+ J\mathbf{A}_q \mathbf{R}_{\rm NBI} \mathbf{A}_q^{\rm H} + \mathcal{N}_o \mathbf{I}.
\end{aligned} \tag{A14}$$

Thus, substituting (A14) into (22) gives rise to

$$\mathrm{SINR}_o(q) = E_1 \left(\mathbf{h}_q^{(1)}\right)^{\rm H} (\mathcal{N}_o \widetilde{\mathbf{R}}_{IN} + J\widetilde{\mathbf{R}}_{NB})^{-1} \mathbf{h}_q^{(1)} \tag{A15}$$

where

$$\widetilde{\mathbf{R}}_{IN} = \sum_{j=2}^{K} \frac{E_j}{\mathcal{N}_o} \sum_{k=-\infty}^{\infty} \widetilde{\mathbf{h}}_q^{(j)}[n-k] \left(\widetilde{\mathbf{h}}_q^{(j)}[n-k]\right)^{\rm H} + \mathbf{I} \tag{A16}$$

$$\widetilde{\mathbf{R}}_{NB} = \mathbf{A}_q \mathbf{R}_{\rm NBI} \mathbf{A}_q^{\rm H}. \tag{A17}$$

Since $\widetilde{\mathbf{R}}_{\rm IN}$ and $\widetilde{\mathbf{R}}_{\rm NB}$ are positive definite and positive semidefinite, respectively, the simultaneous diagonalization [21] of $\widetilde{\mathbf{R}}_{\rm IN}$ and $\widetilde{\mathbf{R}}_{\rm NB}$ can be performed, that is, there exists an $M \times M$ matrix $\mathbf{U}$ such that

$$\mathbf{U}^{\rm H} \widetilde{\mathbf{R}}_{IN} \mathbf{U} = \mathbf{I} \tag{A18}$$

$$\mathbf{U}^{\rm H} \widetilde{\mathbf{R}}_{NB} \mathbf{U} = \widetilde{\mathbf{\Lambda}} \tag{A19}$$

$$\begin{aligned}
r &= \operatorname{rank}(\widetilde{\mathbf{R}}_{NB}) \\
&= \operatorname{rank}(\mathbf{U}^{\rm H} \widetilde{\mathbf{R}}_{NB} \mathbf{U})
\end{aligned} \tag{A20}$$

where $\widetilde{\mathbf{\Lambda}}$ is a diagonal matrix where the kth diagonal entry $\widetilde{\lambda}_{q,k}$ is the kth eigenvalue of $\widetilde{\mathbf{R}}_{IN}^{-1} \widetilde{\mathbf{R}}_{NB}$. Let

$$\mathbf{U} = [\mathbf{u}_{q,1}, \mathbf{u}_{q,2}, \ldots, \mathbf{u}_{q,M}]. \tag{A21}$$

Using (A18)–(A20), $\mathrm{SINR}_o(q)$ given by (A15) can be further simplified as follows:

$$\begin{aligned}
\mathrm{SINR}_o(q) &= E_1 \left(\mathbf{h}_q^{(1)}\right)^{\rm H} (\mathcal{N}_o \widetilde{\mathbf{R}}_{IN} + J\widetilde{\mathbf{R}}_{NB})^{-1} \mathbf{h}_q^{(1)} \\
&= E_1 \left(\mathbf{h}_q^{(1)}\right)^{\rm H} \mathbf{U} (\mathcal{N}_o \mathbf{I} + J\widetilde{\mathbf{\Lambda}})^{-1} \mathbf{U}^{\rm H} \mathbf{h}_q^{(1)} \\
&= \sum_{k=1}^{r} \frac{\left|\left(\mathbf{h}_q^{(1)}\right)^{\rm H} \mathbf{u}_{q,k}\right|^2}{\left(\frac{J}{C_1}\right)\left(\frac{1}{T_c P}\right)\widetilde{\lambda}_{q,k} + \left(\frac{\mathcal{N}_o}{E_1}\right)} \\
&\quad + \frac{E_1}{\mathcal{N}_o} \sum_{k=r+1}^{M} \left|\left(\mathbf{h}_q^{(1)}\right)^{\rm H} \mathbf{u}_{q,k}\right|^2
\end{aligned} \tag{A22}$$

which is exactly (48).

References

[1] Federal Communications Commission, "First report and order in the matter of revision of part 15 of the Commission's rules regarding ultra-wideband transmission systems," ET-Docket 98-153, FCC 02-48, Apr. 22, 2002.

[2] S. Roy, J. R. Foerster, V. S. Somayazulu, and D. G. Leeper, "Ultra-wideband radio design: The promise of high-speed, short-range wireless connectivity," *Proc. IEEE*, vol. 92, no. 2, pp. 295–311, Feb. 2004.

[3] M. Abou-Khousa, M. El-Tarhuni, and A. Ghrayeb, "A novel finger assignment algorithm for RAKE receivers in CDMA systems," in *Proc. IEEE Int. Conf. Commun.*, Paris, France, Jun. 20–24, 2004, vol. 5, pp. 2516–2520.

[4] M. Z. Win, G. Chrisikos, and N. R. Sollenberger, "Performance of RAKE reception in dense multipath channels: Implications of spreading bandwidth and selection diversity order," *IEEE J. Sel. Areas Commun.*, vol. 18, no. 8, pp. 1516–1525, Aug. 2000.

[5] D. Cassioli, M. Z. Win, F. Vatalaro, and A. F. Molisch, "Performance of low complexity RAKE reception in a realistic UWB channel," in *Proc. IEEE Int. Conf. Commun.*, New York, Apr. 28–May 2, 2002, vol. 2, pp. 763–767.

[6] A. G. Klein, D. R. Brown, III, D. L. Goeckel, and C. R. Johnson, "Rake reception for UWB communication systems with intersymbol interference," in *Proc. IEEE Workshop Signal Process. Advances Wireless Commun.*, Rome, Italy, Jun. 15–18, 2003, pp. 244–248.

[7] N. Boubaker and K. B. Letaief, "A low complexity MMSE-RAKE receiver in a realistic UWB channel and in the presence of NBI," in *Proc. IEEE Wireless Commun. Networking Conf.*, New Orleans, LA, Mar. 16–20, 2003, vol. 1, pp. 233–237.

[8] S. S. Tan, B. Kannan, and A. Nallanathan, "Performance of UWB multiple access impulse radio systems in multipath environment with antenna array," in *Proc. IEEE Global Telecommun. Conf.*, San Francisco, CA, Dec. 1–5, 2003, vol. 4, pp. 2182–2186.

[9] X. Wang and H. V. Poor, "Space-time multiuser detection in multipath CDMA channels," *IEEE Trans. Signal Process.*, vol. 47, no. 9, pp. 2356–2374, Sep. 1999.
[10] J. Ramos, M. D. Zoltowski, and H. Lui, "Low-complexity space-time processor for DS-CDMA communications," *IEEE Trans. Signal Process.*, vol. 48, no. 1, pp. 39–52, Jan. 2000.
[11] S. Tanaka, M. Sawahashi, and F. Adachi, "Pilot symbol-assisted decision-directed coherent adaptive array diversity for DS-CDMA mobile radio reverse link," *IEICE Trans. Fundamentals*, vol. E80-A, no. 12, pp. 2445–2454, Dec. 1997.
[12] F. Rashid-Farrokhi, L. Tassiulas, and K. J. R. Liu, "Joint opitmal power control and beamforming in wireless networks using antenna arrays," *IEEE Trans. Commun.*, vol. 46, no. 10, pp. 1313–1324, Oct. 1998.
[13] S. Buzzi, M. Lops, and A. M. Tulino, "MMSE RAKE reception for asynchronous DS/CDMA overlay systems and frequency-selective fading channels," in *Wireless Personal Communications*. Norwell, MA: Kluwer, 2000, pp. 295–318.
[14] A. Shah and A. M. Haimovich, "Performance of space time receiver architectures for CDMA overlay of narrowband waveforms for personal communication systems," in *Proc. IEEE Int. Conf. Commun.*, Montreal, QC, Canada, Jun. 8–12, 1997, vol. 1, pp. 314–318.
[15] A. M. Haimovich and A. Shah, "The performance of space time processing for suppressing narrowband interference in CDMA communications," in *Wireless Personal Communications*. Norwell, MA: Kluwer, 1998, pp. 233–255.
[16] J. G. Proakis, *Digital Communications*, 4th ed. New York: McGraw-Hill, 2001.
[17] V. Tripathi, A. Mantravadi, and V. V. Veeravalli, "Channel acquisition for wideband CDMA signals," *IEEE J. Sel. Areas Commun.*, vol. 18, no. 8, pp. 1483–1494, Aug. 2000.
[18] L. Zhao and A. M. Haimovich, "Performance of ultra-wideband communications in the presence of interference," *IEEE J. Sel. Areas Commun.*, vol. 20, no. 12, pp. 1684–1691, Dec. 2002.
[19] H. V. Poor and X. Wang, "Code-aided interference suppression for DS/CDMA communications—Part I: Interference suppression capability," *IEEE Trans. Commun.*, vol. 45, no. 9, pp. 1101–1111, Sep. 1997.
[20] IEEE P802.15 Working Group for WPANs, Channel Modeling Sub-Committe Report Final IEEE P802.15-02/368r5-SG3a, Dec. 2002.
[21] H. Stark and J. W. Woods, *Probability and Random Processes With Applications to Signal Processing*, 3rd ed. Upper Saddle River, NJ: Prentice-Hall, 2002.

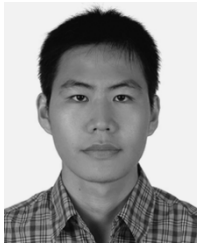

Tsung-Hui Chang was born in Taiwan, R.O.C., on March 4, 1981. He received the B.S. degree from National Tsing-Hua University, Hsinchu, Taiwan, R.O.C., in 2002, where he is currently working toward the Ph.D. degree.

His research interests include statistical signal processing, digital signal processing, and wireless communications.

Chong-Yung Chi (S'83–M'83–SM'89) was born in Taiwan, R.O.C., on August 7, 1952. He received the B.S. degree from the Tatung Institute of Technology, Taipei, Taiwan, R.O.C., in 1975, the M.S. degree from the National Taiwan University, Taipei, Taiwan, R.O.C., in 1977, and the Ph.D. degree from the University of Southern California, Los Angeles, in 1983, all in electrical engineering.

From July 1983 to September 1988, he was with the Jet Propulsion Laboratory, Pasadena, CA, where he was involved with the design of various spaceborne radar remote sensing systems including radar scatterometers, SARs, altimeters, and rain mapping radars. From October 1988 to July 1989, he was a Visiting Specialist with the Department of Electrical Engineering, National Taiwan University. He has been a Professor with the Department of Electrical Engineering since August 1989 and the Institute of Communications Engineering (ICE) since August 1999 (also the Chairman of ICE for August 2002–July 2005), National Tsing Hua University, Hsinchu, Taiwan, R.O.C. He was a Visiting Researcher with the Advanced Telecommunications Research (ATR) Institute International, Kyoto, Japan, May and June 2001. He coauthored, with C.-C. Feng, C.-H. Chen, and C.-Y. Chen, a technical book entitled *Blind Equalization and System Identification* (Springer-Verlag, 2006) and more than 120 technical papers in radar remote sensing, system identification and estimation theory, deconvolution and channel equalization, digital filter design, spectral estimation, higher order statistics-based signal processing, and wireless communications. His current research interests include signal processing for wireless communications, statistical signal processing, and digital signal processing and their applications.

Dr. Chi is a member of European Association for Signal Processing and an active member of the Chinese Institute of Electrical Engineering. He has been a Technical Program Committee member for more than a dozen IEEE sponsored workshops, symposiums, and conferences on signal processing and wireless communications, including coorganizer and a General Cochairman of the 2001 IEEE Signal Processing Workshop on Signal Processing Advances in Wireless Communications (SPAWC-2001). He was also the Chair of the Information Theory Chapter of IEEE Taipei Section (7/2001–6/2003). Currently, he is an Associate Editor for the IEEE TRANSACTIONS ON SIGNAL PROCESSING, an Associate Editor for the IEEE TRANSACTIONS ON CIRCUITS AND SYSTEMS II—EXPRESS BRIEFS, and an Editorial Board Member of *The EURASIP Journal on Applied Signal Processing*), a member of the Editorial Board of the *EURASIP Signal Processing Journal*, and a member of the Technical Committee on Signal Processing Theory and Methods for the IEEE Signal Processing Society.

Yu-Jung Chang received the B.S. degree from Tamkang University, Taipei, Taiwan, R.O.C., in 2003, and the M.S. degree from National Tsing Hua University, Hsinchu, Taiwan, R.O.C., in 2005.

Since January 2006, he has been with Accton Inc., Hsinchu, where he works on design and implementation of network switches. His research interests include digital signal processing and wireless communications.